Two Approaches to Quantification of Force Networks in Particulate Systems

Rituparna Basak[1]; C. Manuel Carlevaro[2]; Ryan Kozlowski[3]; Chao Cheng[4]; Luis A. Pugnaloni[5]; Miroslav Kramár[6]; Hu Zheng[7]; Joshua E. S. Socolar[8]; and Lou Kondic[9]

Abstract: The interactions between particles in dense particulate systems are organized in force networks, mesoscale features that influence the macroscopic response to applied stresses. The detailed structure of these networks is, however, difficult to extract from experiments that cannot resolve individual contact forces. In this study, we showed that certain persistent homology (PH) measures extracted from data accessible to experiment are strongly correlated with the same features extracted from the full contact force network. We performed simulations known to accurately model experiments on an intruder being pushed through a two-dimensional (2D) granular layer and compared PH properties of full contact force networks and networks constructed using only the sum of the normal forces on each grain. We found that the main features were highly correlated, suggesting that data commonly available in experiments are sufficient for quantifying the structure of force networks in evolving granular systems. **DOI: 10.1061/(ASCE)EM.1943-7889.0002003.**

Author keywords: Particulate systems; Force networks; Persistent homology.

Introduction

In recent years, a significant amount of research has been carried out on the topic of relating interparticle forces in static, compressed, or sheared dry or wet granular systems with the system-wide response; see Behringer and Chakraborty (2018) for a recent review. This body of research has established clear connections between particle-scale interactions, mesoscopic structures loosely referred to as force networks, and macroscale system properties. Therefore, in order to understand the properties of a system as a whole, it is crucial to understand and quantify the properties of the underlying force networks, that is, the force field that describes the interparticle interactions.

The connection between the microscale (particle–particle interactions), mesoscale (which can be related to the scale introduced by force networks, spanning roughly 5–15 particles), and macroscale has been considered extensively in the literature (see e.g., Radjai et al. 1996; Azéma and Radjaï 2012; Nicot et al. 2017; Kawamoto et al. 2018; Li et al. 2019; Liu et al. 2020). More force network–centered analyses have been carried out as well, using a variety of methods. These have included force network ensemble analysis (Snoeijer et al. 2004; Tighe et al. 2010; Sarkar et al. 2013), statistics-based methods (Peters et al. 2005; Tordesillas et al. 2010, 2012; Bo et al. 2014), network analysis (Bassett et al. 2012; Walker and Tordesillas 2012; Tordesillas et al. 2015; Giusti et al. 2016), and topological data analysis—in particular, persistent homology (PH) (Arévalo et al. 2010, 2013; Ardanza-Trevijano et al. 2014; Kondic et al. 2012, 2016; Kramár et al. 2013, 2014a, b; Pugnaloni et al. 2016). While different methods provide complementary insights, we focused in this study on the PH approach, because it allows for significant data reduction and for formulation of simple but informative measures describing the force networks as well as for comparison of different networks in a dynamic setting. Furthermore, the approach is dimension-independent, being easily applied in both two and three physical dimensions (2D and 3D). Such an approach has been used to discuss force networks in dry and wet (suspensions) systems that were compressed (Kondic et al. 2012; Kramár et al. 2014a), vibrated (Pugnaloni et al. 2016; Kondic et al. 2016), or sheared (Gameiro et al. 2020), as well as for an analysis of the yielding of a granular system during pullout of a buried intruder in 3D (Shah et al. 2020). For example, in Kondic et al. (2016) PH was used to compare the properties of force networks in packings of disks or pentagons; in Gameiro et al. (2020) it was found that a PH-derived measure, total persistence (which we considered in this study as well), correlated very well with the viscosity of a sheared suspension; and in Shah et al. (2020), PH was used to describe how force networks evolve due to the onset of motion of a buried intruder.

While significant progress has been made in quantifying properties of force networks based on data obtained in discrete element simulations, progress in the analysis of experimental data has been slower. The reason for this is that it is difficult to extract information about the forces between particles in experiments.

[1]Dept. of Mathematical Sciences, New Jersey Institute of Technology, Newark, NJ 07102.

[2]Instituto de Física de Líquidos y Sistemas Biológicos, Consejo Nacional de Investigaciones Científicas y Técnicas (Argentina), and Departamento Ing. Mecánica, Universidad Tecnológica Nacional, Facultad Regional La Plata, La Plata 1900, Argentina. ORCID: https://orcid.org/0000-0003-3528-7614

[3]Dept. of Physics, Duke Univ., Durham, NC 27708.

[4]Dept. of Mathematical Sciences, New Jersey Institute of Technology, Newark, NJ 07102.

[5]Departamento de Física, FCEyN, Universidad Nacional de La Pampa, Consejo Nacional de Investigaciones Científicas y Técnicas (Argentina), Santa Rosa, La Pampa 6300, Argentina.

[6]Dept. of Mathematics, Univ. of Oklahoma, Norman, OK 73019.

[7]Dept. of Geotechnical Engineering, College of Civil Engineering, Tongji Univ., Shanghai 200092, China.

[8]Dept. of Physics, Duke Univ., Durham, NC 27708. ORCID: https://orcid.org/0000-0003-0532-7099

[9]Dept. of Mathematical Sciences, New Jersey Institute of Technology, Newark, NJ 07102 (corresponding author). ORCID: https://orcid.org/0000-0001-6966-9851. Email: kondic@njit.edu

Note. This manuscript was submitted on February 23, 2021; approved on June 26, 2021; published online on September 11, 2021. Discussion period open until February 11, 2022; separate discussions must be submitted for individual papers. This paper is part of the ***Journal of Engineering Mechanics***, © ASCE, ISSN 0733-9399.

Significant progress in this direction has been obtained using photoelastic systems in which, based on the photoelastic response on the single-particle scale, one can extract information about the forces at particle–particle contacts (Zadeh et al. 2019). Such measurements, however, are computationally expensive and require high-resolution input data so that the contact forces can be accurately extracted across a broad range of forces. Moreover, particles containing flat edges lead to additional complications. Very often, the data do not meet the aforementioned requirements, and the reconstruction cannot be carried out; instead, semiquantitative or qualitative measures must be utilized. Depending on the quality of the data, one can use either the gradient-squared (G^2) method (Zadeh et al. 2019; Howell et al. 1999) to extract the sum of the magnitudes of the forces on a particle (Zhao et al. 2019) or one can simply analyze the integrated intensities of raw photoelastic images of each grain to explore whether the available information is sufficient to extract meaningful data. The approach based on G^2 data has been used in the context of shear jamming experiments (Dijksman et al. 2018), while the latter approach has been used to analyze granular impact (Takahashi et al. 2018) and the stick-slip dynamics of a slider on top of a granular bed (Cheng et al. 2021). These analyses were carried out using PH-based tools, which provided insightful information about the role of force networks in the systems considered. For example, in Dijksman et al. (2018), it was found that a precise comparison between discrete-element method (DEM) simulations and experimental force networks could be reached by perturbing (for the purpose of PH computations) the forces between the particles computed in simulations by white noise to mimic experimental noise. In Cheng et al. (2021), it was discovered that the PH-based measures showed clear correlations between the evolution of force networks and the stick-slip dynamics of a slider moving on top of a granular medium.

The analyses of the aforementioned force networks appear to establish meaningful connections between particle scale physics and macroscopic system response. It should be emphasized, however, that complete data on interparticle forces were not available for study due to experimental limitations. Instead, the topological analyses utilized image intensities that reflected only partial information, such as the total stress on each grain. This raises the following question: How accurate is the analysis based on incomplete data? Consider, for example, a study of granular impact dynamics (Takahashi et al. 2018), in which an analysis of photoelastic images led to the conclusion that loops in the force network played an important role in slowing down the intruder. If more detailed information about individual contacts were available for constructing the force networks, would a loop analysis still support that conclusion?

Answering the outlined question requires having complete information regarding particle–particle forces, computing relevant results, and comparing the results to results obtained based on incomplete information. To be able to carry out such a project, two necessary conditions need to be met: (1) one should be able to compare the results obtained based on different sets of data, and (2) one should be able to obtain information about the particle–particle forces. Regarding (2), information about particle–particle forces is difficult and costly to obtain in experiments, as discussed previously. The simpler approach is to consider DEM simulations and construct two networks for comparison: one formed from a full set of contact forces and the other from the total normal force on each particle. Regarding (1), it is convenient to use the PH-based approach, because the corresponding analysis can be carried out both using the information about the force networks based on particle–particle contact forces and based on the total force on each particle.

In the present paper, we illustrate the outlined approach in the context of recent experiments and simulations that considered the intermittent dynamics of an intruder in an annular Couette geometry discussed in our recent work (Kozlowski et al. 2019; Carlevaro et al. 2020). Fig. 1 shows the setup of the experiment motivating the system studied by simulations in the present work, and Fig. 2 presents photoelastic images acquired in experiments as well as processed images of force networks extracted using the G^2 method. The latter were produced from measurements of the average of the square of the intensity gradient over the pixels with each grain, then creating an image in which each pixel in the grain is assigned the average value. In this system, a bidisperse monolayer of around 1,000 photoelastic disks (or pentagons) was confined to an annular region by fixed boundaries lined with ribbed rubber to prevent slipping at the boundaries. In one set of experiments described in Kozlowski et al. (2019), disks were floated on a water–air interface to remove friction with the glass base, while in other experiments with disks and pentagons, the particles had basal friction. An intruding disk was pushed in the counterclockwise azimuthal direction (at a fixed radius) by a torque spring. One end of the torque spring was coupled to the intruder, while the other end was driven at a fixed angular rate ω. By using a spring stiffness that was far smaller than the grain material stiffness, stick-slip dynamics was studied. Cameras above the system tracked grains and, by use of a dark-field polariscope (Daniels et al. 2017), visualized grain-scale stresses, as demonstrated in Fig. 2. A detailed analysis of the insights of PH into these experimental data will be presented elsewhere; the focus of the present work is to study this system using simulations that are not limited by experimental resolution and in which exact forces are known.

In brief, the goal of the present work was to compare the properties of the force networks formulated using the contact forces (FC) and the ones formulated from the total force on each particle (FP) and to discuss whether the topological measures computed for FP accurately described FC, in a manner that will be made precise in

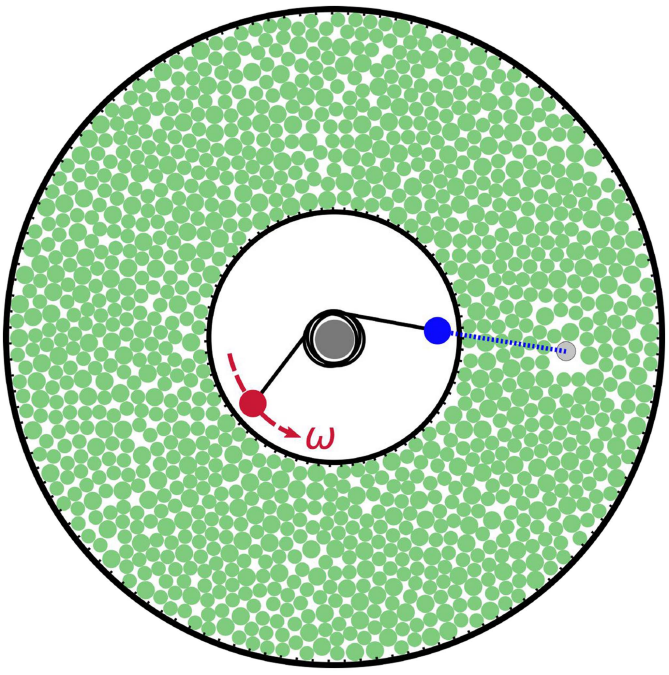

Fig. 1. Experimental setup serving as a motivation for the present work: the intruder is coupled to one end of a torque spring (dark); the other end of the torque spring (dashed line) is rotated at fixed angular velocity ω. The grains fill an annular channel with rough boundaries to prevent slipping at the boundaries.

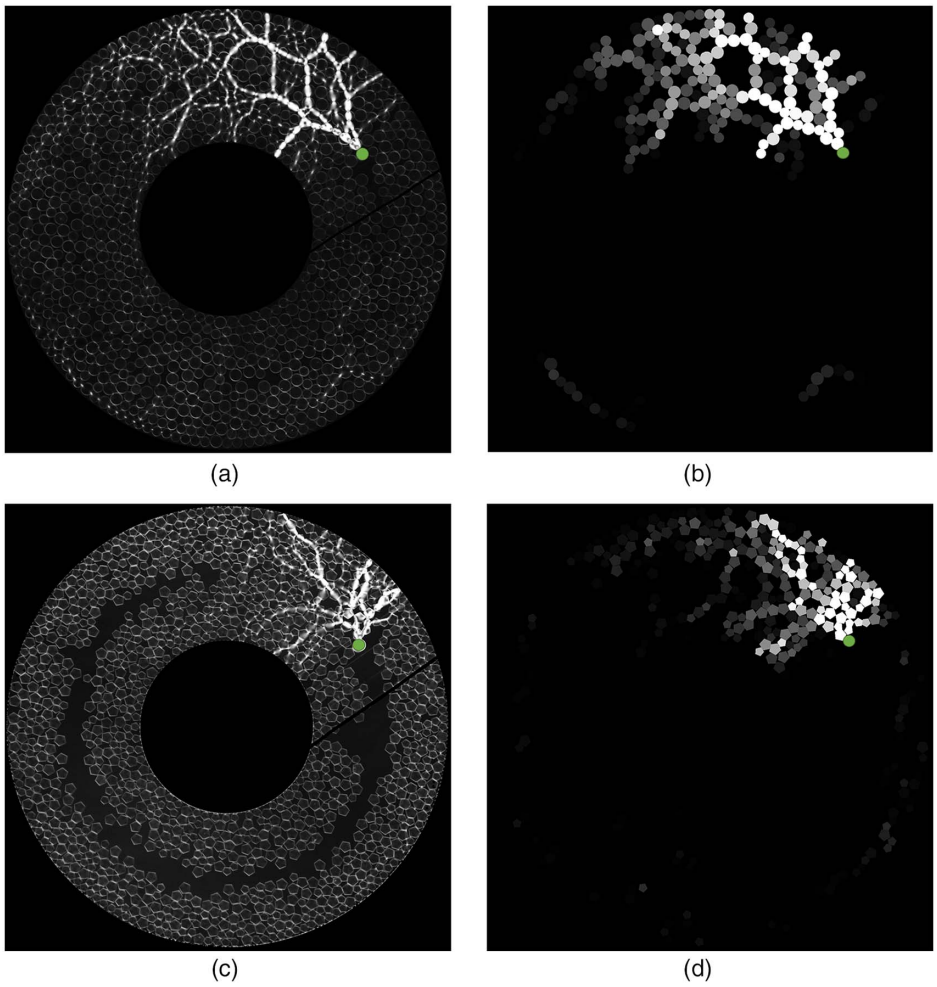

Fig. 2. (a) Disks, photoelastic image; (b) disks, G^2; (c) pentagons, photoelastic image; and (d) pentagons, G^2. (a) and (c) are experimental photoelastic images and (b) and (d) are processed images of the same configurations showing G^2 per grain. (a) and (b) correspond to a packing of disks and (c) and (d) to a packing of pentagons. The intruder is the shaded particle at the endpoint of the open channel, from which the force network originates.

the "Results" section below. For simplicity, in the present work we consider only the normal contact forces for the purpose of defining both FC and FP networks. The total force on a particle is meant here as the sum of the magnitudes of normal forces.

The remainder of this paper is structured as follows. In the methods section, we discuss the simulated systems and topological data analysis methods used in this study. This section also includes a brief discussion of a toy example that illustrates how the PH analysis of the data is carried out. In the results section, we present the topological measures quantifying the force networks. We considered both the data obtained in the stick-slip regime, in which the intruder was essentially static for significant periods of time, and in the clogging regime, in which the intruder was rarely at rest. The computations were carried out for both disks and pentagons so that we could also obtain some insight into the influence of particle shape on the correlations between the FP and FC networks.

Methods

Simulations

The simulations were implemented using the technique discussed in Carlevaro et al. (2020). Here we provide a brief overview for completeness; the interested reader is referred to that paper for all the details. Our model considered the grains to be (hard) rigid impenetrable 2D objects (disks or regular pentagons) that experience both normal and tangential forces when they are in contact with each other or the walls. The 2D particles slide on a flat frictional substrate inside an annulus defined by rigid walls. An intruder particle is dragged through the granular system in a circle (concentric with the annular cell boundaries) by pulling it via a soft torsion spring at a very low speed. The interaction with the substrate was defined by dynamic and static sliding friction coefficients, but rotational friction was set to zero. Because the model was 2D, we did not allow buckling out of the plane, and we assumed the interparticle forces had no out-of-plane component. Key parameters were chosen to match the values used in the experiments that inspired these simulations, including particle diameters and masses, dimensions of the confining annular region, driving velocity, and torque spring constant (Kozlowski et al. 2019; Carlevaro et al. 2020). We have found that the statistics of the intruder dynamics closely match the experimental results (Carlevaro et al. 2020).

We carried out DEM simulations of the model using the Box2D version 2.3.1 library. The Box2D library uses a constraint solver to handle contacting hard bodies. For this, before each time step, a series of iterations (typically 100) is used to resolve constraints on overlaps and on static friction between bodies through a Lagrange multiplier scheme (Pytlos et al. 2015; Catto 2005).

After resolving overlaps, the force at each detected contact is found by solving the coupled equations of momentum conservation and the definition of restitution coefficient (Pöschel and Schwager 2005). Hence, new linear and angular velocities are assigned to each of the bodies based on all their contact forces. The interaction between particles is defined by a normal restitution coefficient and a friction coefficient (dynamic and static friction coefficients are set to be equal). The equations of motion are integrated through a symplectic Euler algorithm. Solid friction between grains is also handled by means of a Lagrange multiplier scheme that implements the Coulomb criterion. Note that this simulation scheme is different from traditional event-driven simulations of hard particles in which contacts are only instantaneous and collisions are resolved pairwise. Our contacts could last many time steps, as in soft-particle DEM simulations. This hard particle model is much more efficient for solving contact interactions than soft interactions. The approach yields realistic dynamics for granular bodies (Pytlos et al. 2015) with complex shapes. Box2D has been successfully used to study grains under a variety of external drivings (Carlevaro and Pugnaloni 2011; Carlevaro et al. 2020).

Systems consisting of disks were made up of bidisperse mixtures of small disks S (with mass m and diameter d) and large disks L (with mass 1.5625 m and diameter 1.25 d) in a 2.75:1 (S:L) ratio. No crystallization was observed in the simulations for this ratio of particle sizes. We also simulated a bidisperse mixture of pentagons in a 1:1 ratio, with radii 1.086 d and 1.20 d for the small and large sizes, respectively. The time step used to integrate the Newton–Euler equations of motion was $\delta t = 0.0278\sqrt{d/g}$, where g is the acceleration of gravity acting in the direction perpendicular to the substrate. The restitution coefficient was set to $\varepsilon = 0.05$, and the friction coefficient μ was set to 1.2 for the grain–grain and grain–wall interactions. The static and dynamic friction coefficients with the substrate were set equal to each other and given values of 0.36 (frictional substrate) or 0 (frictionless substrate). The particles were contained in a 2D Couette cell formed by two concentric rings of radii 8.81 d and 22.80 d. These rings were made up of small equilateral triangles facing inward (toward the annular channel) to prevent the slippage of particles at the boundaries.

The intruder was a disk with $d_i = 1.25\ d$ and was constrained to move on a circular trajectory midway between the inner and outer rings. The intruder could interact with any other grain in the system but did not interact with the base (i.e., it had no basal friction). It was pulled by a torsion spring with a spring constant of 3591.98 mgd/rad. One end of this spring was attached to the intruder; the other was driven at a constant angular velocity of $0.00432\sqrt{g/d}$. This spring could only pull the intruder; no force was applied when the spring became shorter than its equilibrium length.

During the simulations, the intruder displayed stick-slip dynamics and the particles in the system developed a force network during the sticking periods that fully rearranged after each slip event. These force networks resembled the ones observed in experiments (see Fig. 2). We saved the contact forces (normal and tangential components) for every single contact in the system for further analysis through persistent homology (discussed in the following). Contact forces were calculated from the impulses (normal and tangential) after resolving each contact collision. In the case of pentagonal particles, the side-to-side contacts were defined by two points and two forces (one at each point selected along the contact line). The total force at the contact was obtained as the vector sum of these two forces. As mentioned previously, for the network analysis we focused on the normal forces at each contact.

Extracting Force Networks: Contact Forces and Particle Forces

In this section, we present a toy example that clarifies the definitions of the contact force and particle force networks. In the following section these networks are used to demonstrate basic properties of persistence diagrams. Roughly speaking, both force networks are defined by a real-valued function on a contact network created by the particles. In this study, we focused on the normal forces between the particles, so the aforementioned real-valued function should be thought of as a normal force between the particles. We start by considering an ensemble of particles p_i, $i = 1, \ldots, N$. The contact network CN is a graph with vertices v_i, $i = 1, \ldots, N$ corresponding to particle centers. An edge $\langle v_i, v_j \rangle$ is present in the contact network if the particles p_i and p_j are in contact.

To define the force networks, we must assign real values to both the vertices and edges of the CN graph. If we know the forces between the particles, then it is natural to define the $f_{\mathrm{FC}}(\langle v_i, v_j \rangle)$ to be the magnitude of the contact force between particles p_i and p_j. For reasons that will be explained subsequently, we extend the definition of f_{FC} to the vertices, so that the value at vertex v_i is the maximum value of f_{FC} on the edges that contain v_i. Fig. 3(a) shows a simple example of a possible contact force (FC) network. In this toy example we specify the force values by hand; for the data discussed in the results section, these forces were obtained from simulations.

If only the total force on each particle is known, it is natural to define a particle force (FP) network with $f_{\mathrm{FP}}(v_i)$ equal to the total force experienced by particle p_i—that is, the sum of the normal (as discussed previously) forces at the contacts of p_i with its neighbor p_j. Here, for reasons that will be explained subsequently, we expand the definition of f_{FP} to the edges by $f_{\mathrm{FP}}(\langle v_i, v_j \rangle = \min(f_{\mathrm{FP}}(v_i), f_{\mathrm{FP}}(v_j))$. Figs. 3(b and c) show an example. Note that the forces on the vertices are defined by the sums of the forces on the edges from Fig. 3(a); these forces are shown in Fig. 3(b). Then, the force on each edge $\langle v_i, v_j \rangle$ is assigned as the minimum of total forces on p_i and p_j. These values are shown in Fig. 3(c).

Persistent homology provides a precise quantification of the structure of the force networks for all threshold values θ of the force. For the FC network, the persistent homology describes how the topological structure of the superlevel sets changes with θ. In the present context, a superlevel set corresponds to all the edges that are assigned a force stronger than the specified threshold θ or, in more precise terms, $\mathrm{FC}(\theta) = \{\sigma \in_{\mathrm{CN}} : f_{\mathrm{FC}}(\sigma) \geq \theta\}$. Similarly, for the FP network, the superlevel sets are given by $\mathrm{FP}(\theta) = \{\sigma \in_{\mathrm{CN}} : f_{\mathrm{FP}}(\sigma) \geq \theta\}$. In order to use persistent homology, the families of superlevel sets $\mathrm{FC}(\theta)$ and $\mathrm{FP}(\theta)$ must satisfy the following property: If the edge $\langle v_i, v_j \rangle$ belongs to a given superlevel set, then both vertices v_i and v_j must belong to this set as well. This governs our choice for extending the functions f_{FC} and f_{FP}.

To relate these networks to ones that are obtained in experiments or simulations of granular systems, we note that the FC network requires as an input all the contact forces, which are difficult to obtain in experiments. A key point, as mentioned previously, is that in experiments the FP network can be obtained much more easily than the FC network.

Our toy example illustrates that the structures of $\mathrm{FC}(\theta)$ and $\mathrm{FP}(\theta)$ can be very different. For example, the top two layers of particles are connected by edges with much smaller values in Fig. 3(a) than in Fig. 3(c). It is not clear how to identify meaningful similarities and differences between snapshots of the two networks. Instead, the natural question is whether the time

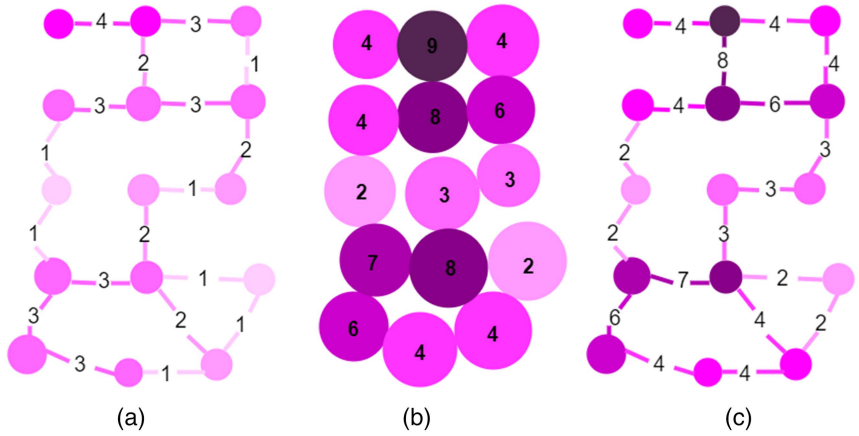

Fig. 3. Toy example illustrating contact force (FC) and particle force (FP) networks: (a) FC network; the values of the forces at each age are prescribed (as shown by the numbers); (b) FP network, Representation 1; the number assigned to each particle shows the total force on that particle (vertex), obtained by summing up the forces on the edges from (a); and (c) FP network, Representation 2, the associated network showing the forces on the edges connecting the particles in (b) as described in the text. Clearly, the FC (a) and the FP (c) networks are different. Note that the FP network shown in (c) does not require the information from (a) as long as the total force on each particle [as shown in (b)] is known.

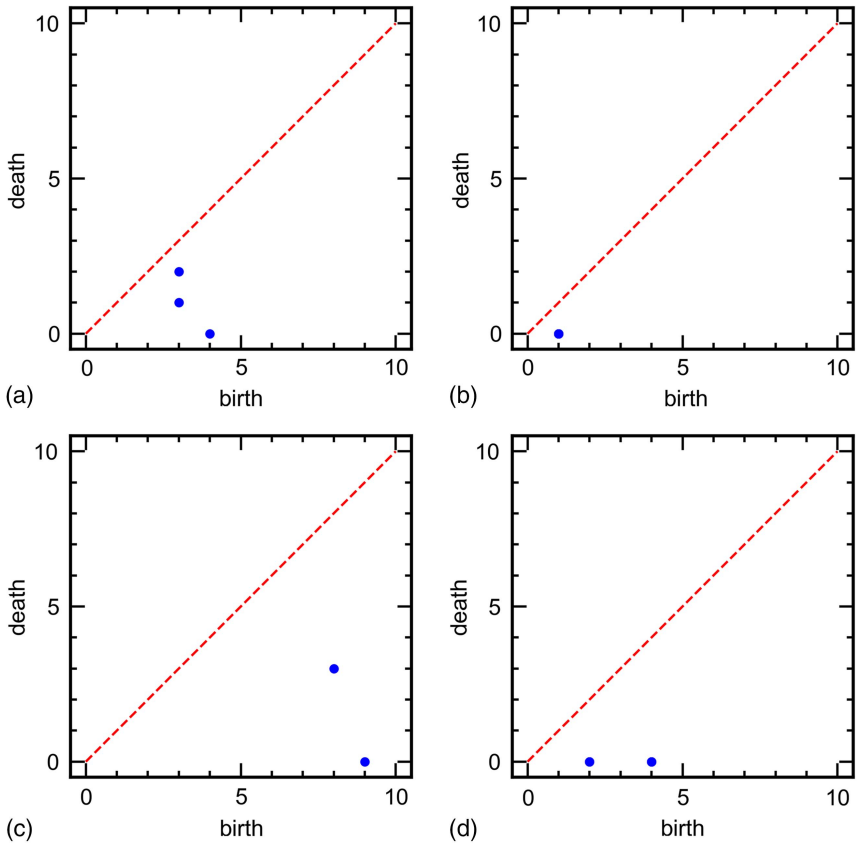

Fig. 4. Persistence diagrams, PDs, corresponding to the FC and FP networks from Fig. 3: (a) FC, β_0; (b) FC, β_1; (c) FP, β_0; and (d) FP, β_1.

evolution of one network is closely correlated to the evolution of the other. We address this question through persistent homology.

Persistent Homology Tools

For the present purposes, one can think of persistent homology as a tool for describing the structure of weighted networks such as FC(θ) and FP(θ). The reader is referred to Shah et al. (2020) for a more detailed overview of the application of PH to dense granular matter from a physics point of view and to Kramár et al. (2016) for a more in-depth presentation. For our present purposes, we briefly outline the main ideas and illustrate them with the foregoing toy example. We focus on the use of PH to quantify the differences between the considered networks.

Given a weighted network, PH assigns to it two persistence diagrams PD β_0 and PD β_1, which describe how the structure of the superlevel set changes with the threshold θ. PD β_0 encodes how distinct connected components in the superlevel set appear and

then merge as θ decreases. The appearance and merging of these components is precisely encoded by the birth and death coordinates of the points in PD β_0. A birth occurs when an edge that is not connected to any existing edge is added to the superlevel set. As θ decreases, a cluster of connected edges grows from the birth edge. A death occurs when a newly added edge connects two existing clusters, and we define the cluster with the most recent birth coordinate to be the one that dies. To put this in context, in a granular system, high threshold values correspond to strong forces, the components correspond (in a vague sense) to so-called force chains, and merging corresponds to force chains connecting with each other at the lower force levels.

Fig. 4(a) illustrates this process using FC(θ) networks from Fig. 3(a). In this network, the first connected component appears for $\theta = 4$ and is represented by the point in PD β_0 with the birth coordinate value 4. There are two more points in this diagram with birth coordinates at 3, and they represent two distinct components that appear at this threshold, one at the bottom of the network and the other consisting of the edges in the second layer from the top. The latter component merges with the top layer at $\theta = 2$, and it disappears (dies) at this value so that the lifetime of this component is described by the point $(3, 2) \in$ PD β_0. The bottom component merges with the rest of the network at $\theta = 1$ and is represented by $(3, 1) \in$ PD β_0. The first component that appeared for $\theta = 4$ is present for all values of θ and is identified by the point $(4, 0) \in$ PD β_0. To once again put this in context, note that the points in the diagram can be related to the common (even if not always precisely defined) concept of force chains. The birth and death coordinates indicate the force levels at which different force chains form and merge. A point far from the diagonal represents a distinct component that is isolated (in terms of particle/contact forces) and merges with the rest of the system only at low force thresholds. A point close to the diagonal corresponds to a component that emerges at a given threshold but soon merges at a slightly lower threshold with a neighboring component. These short-lived components can be considered noise, because they may correspond to arbitrarily small variations in particle/contact forces.

The persistence diagram PD β_0 shown in Fig. 4(c) for the FP network describes the appearance and disappearance of the connected components in the network FP(θ) depicted in Fig. 3(c). Clearly, this diagram is different from the one for FC(θ) extracted from the same system. As mentioned previously, the high values in the FP network are attained at places where force chains come close to each other or intersect. As indicated by the presence of two points in PD_0, there are two distinct places in the FP network where this happens, as seen in Figs. 3(b and c).

PD β_1 describes the appearance of loops in the superlevel sets. If a loop appears at a given threshold θ_1, then it is present for all values $\theta \le \theta_1$ and is represented by the point $(\theta_1, 0) \in$ PD β_1; see Kramár et al. (2014b) for a more precise discussion of this concept. For the FC network shown in Fig. 3(c), there are four loops that appear in PD β_1 at $\theta_1 = 1$, as shown in Fig. 4(b), and they are represented by four copies (on top of each other) of the point (1, 0). For the FP network, there are four loops. Two appear at the top right and the bottom left of the network at $\theta_1 = 4$ and are represented in PD β_1 by two copies of the point (4, 0). The other two are born

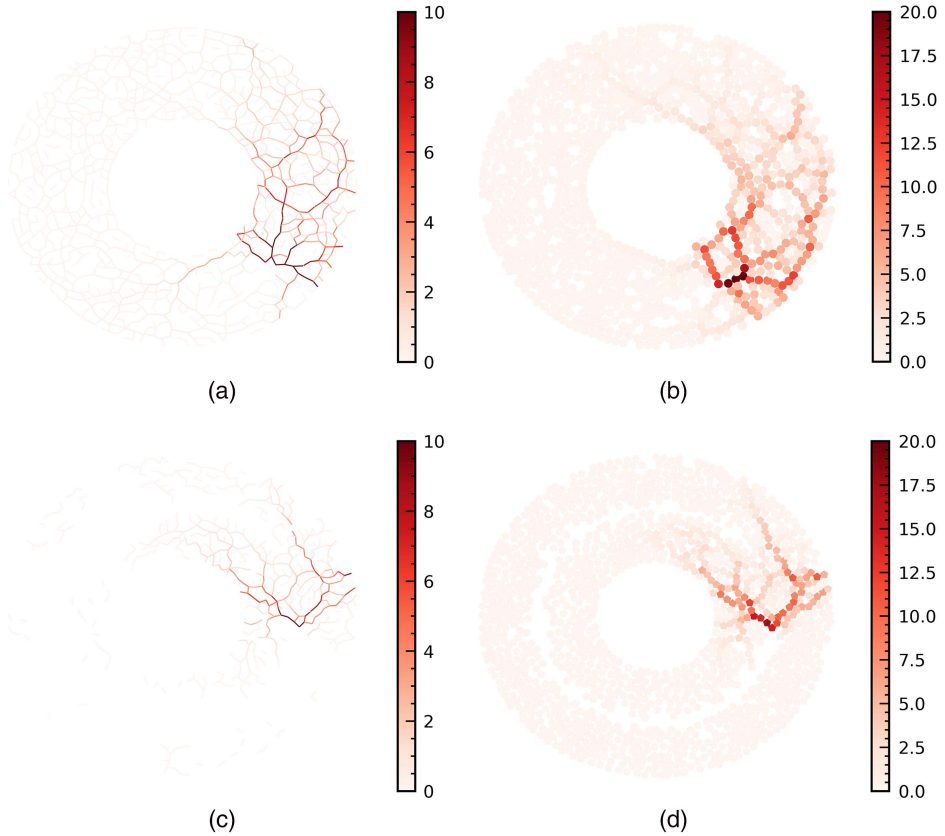

Fig. 5. Snapshot of force networks obtained from simulation results, for (a and b) disks at packing fraction $\phi = 0.78$; and (c and d) pentagons at $\phi = 0.62$. The information obtained from simulations is the same in (a and b) and (c and d), but in (a and c) we use the force contact (FC) information, while in (b and d) we use the force on a particle (FP) information only. The color bars represent the normalized forces $\hat{f}_{i,j}$ and f_i for the FC and FP networks, respectively, as discussed in the text. Note different range in (a–c) versus (b–d). All results are obtained in the simulations that include basal friction. Animations of the networks are available as Supplemental Materials; see FN-disk and FP-pent.

J. Eng. Mech., 2021, 147(11): 04021100

at $\theta_1 = 2$ and are described by two copies of (2, 0) in PD β_1. As discussed in the context of PD β_0, the PD β_1 diagrams are different for the FC and FP networks.

An important aspect of PH is that it provides information about the force networks at all force levels. Therefore, it does not require separation of a force network into strong and weak networks, although it allows for such classification, as will be discussed in the results section. Each feature of the network can be described by a point (b, d) (where b stands for birth and d stands for death) in one of the persistence diagrams. Moreover, the prominence of a feature is encoded by its lifespan, defined as $b - d$.

The description of a weighted force network in terms of PDs provides a compact but meaningful description of the features of the underlying network. As demonstrated by Fig. 3, the PDs clearly describe the differences between the FC and FP networks. However, the space of PDs is a nonlinear complete metric space (Mileyko et al. 2011), and there is no readily available method for correlating the diagrams. Hence, in the remainder of this paper, we consider several different metrics that can be defined for PDs. Introducing these metrics leads to a further data reduction. One metric considered is the number of points (generators) in a diagram. Another is the lifespan, introduced previously, which describes how long (that is, for how many threshold levels) a point persists. Using a landscape (mountains and valleys) as an analogy, the number of points N_G in PD β_0 corresponds to the number of mountain peaks, and lifespan corresponds to the difference in altitude between a peak and a valley. The lifespans of all points in a persistence diagram can be aggregated into a single number by defining the total persistence TP as the sum of all lifespans. We use both N_G and TP in discussing some properties of the force networks in the considered system.

In our calculations, we defined FC and FP networks based on the normal force between the particles, suitably normalized as discussed in the following. The PH calculations leading to the persistence diagrams were carried out to compute PDs for both FC and FP networks using the software package Gudhi version 3.4.0 (GUDHI 2014). We focused in the present work on the network of interparticle interactions, not including particle–wall forces.

Results

In this section we first discuss the general features of the results for the considered networks, then focus our discussion on the main topic of the paper: the correlations between the contact force and particle force networks.

Contact Force and Particle Force Networks: General Features

Fig. 5 (see also the associated animations in the Supplemental Materials) shows the FC and FP networks obtained from simulations based on the same setup as the experiments depicted in Fig. 2. As discussed previously, these two networks exhibit different features and cannot be directly related. Instead, we show that the time evolution of the PH features of these networks are correlated. We demonstrate this by first extracting the topological measures introduced in the previous section for a large number of networks of both types and then cross-correlating them.

The functions f_{FC} and f_{FP} describing the FC and FP networks were defined as in the previous section. For simplicity, we used the normal forces at each contact to define these networks; considering tangential forces leads to consistent results that, for brevity, we do not discuss in the present paper. In the considered system, the average force between the particles fluctuated significantly during the evolution, so we first normalized the computed forces by their (time-dependent) average. The function f_{FC} describing the force network at a given time was normalized by the mean contact force at that time; the mean was calculated as the sum of $f_{\mathrm{FC}}(e)$ over edges $e \in CN$ divided by the number of edges (only edges carrying nonzero forces are considered). The function f_{FP} was normalized by the sum of its original values $f_{\mathrm{FP}}(v)$ over the vertices (particles) $v \in$ CN divided by the number of vertices, again considering only the vertices (particles) carrying a nonzero force. Fig. 5 shows these

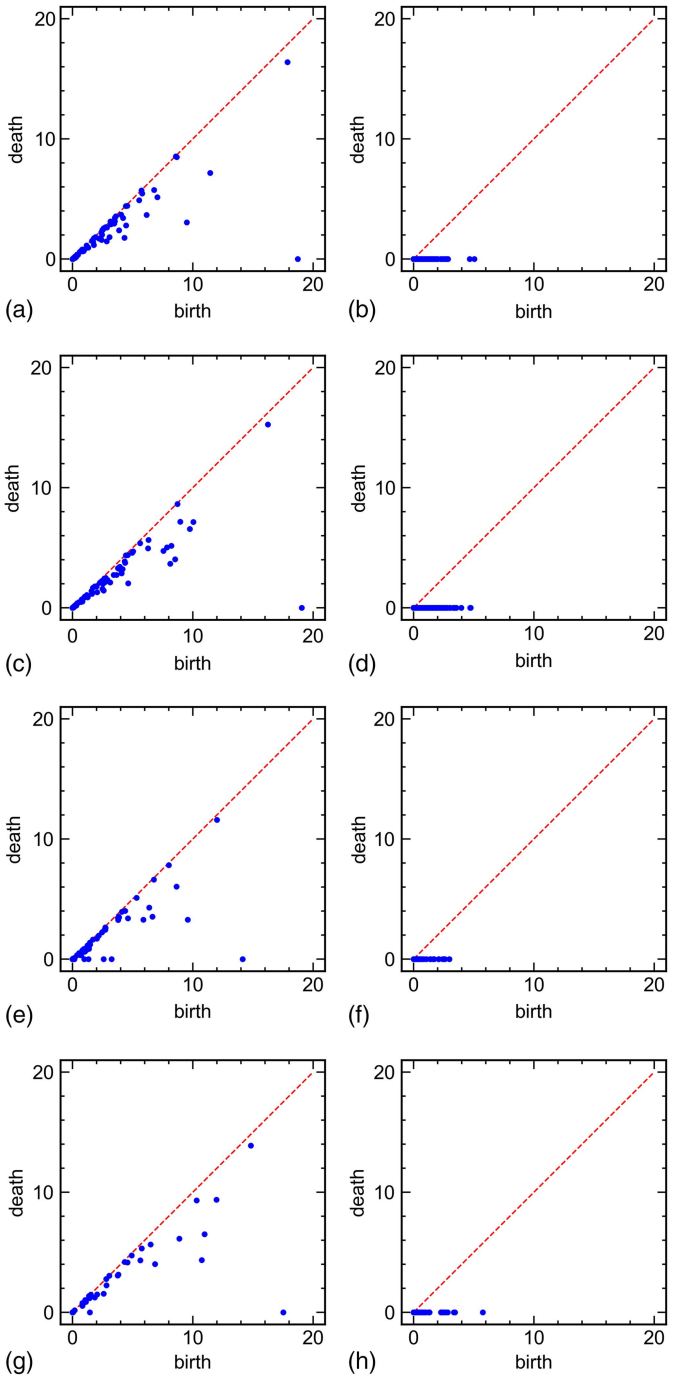

Fig. 6. Persistence diagrams (PDs) corresponding to the networks shown in Fig. 5. Animations of the β_0 PDs for a simulation run are available in the Supplemental materials (see pd-disk and pd-pent): (a) disks, FC, β_0; (b) disks, FC, β_1; (c) disks, FP, β_0; (d) disks, FP, β_1; (e) pentagons, FC, β_0; (f) pentagons, FC, β_1; (g) pentagons, FP, β_0; and (h) pentagons, FP, β_1.

normalized functions. For visualization purposes, each vertex was plotted with the approximate size of the particle whose center it resides at.

The persistence diagrams corresponding to Fig. 5 were computed from the FC(θ) and FP(θ) networks, respectively. Fig. 6 shows the corresponding diagrams (see also the associated animations in the Supplemental Materials, pd-disk and pd-pent). We analyze the properties of a large number of such diagrams in the next section, focusing mostly on two measures, the total persistence and the number of generators N_G. In interpreting the results, it is useful to remember that the generators that are close to the diagonal represent features that persist over only a small range of thresholds and, therefore, are not significant for the purpose of identifying robust features, because they may be a consequence of only minor changes in the interparticle forces. We will see subsequently that excluding these insignificant features may help considerably in relating the FC and FP networks.

Comparison of Contact Force and Particle Force Networks

Having specified how the PDs for the two types of networks were computed, we now proceed with the comparison of the large number of diagrams extracted from time-dependent simulation data. In our analysis, we considered four systems, with parameter choices motivated by our previously reported results on intruder dynamics (Carlevaro et al. 2020). First, we discuss the results obtained for disks in simulations that included the basal friction (friction with the substrate) for packing fraction $\phi = 0.78$; then we continue with pentagons for $\phi = 0.62$. In such systems, for the simulation

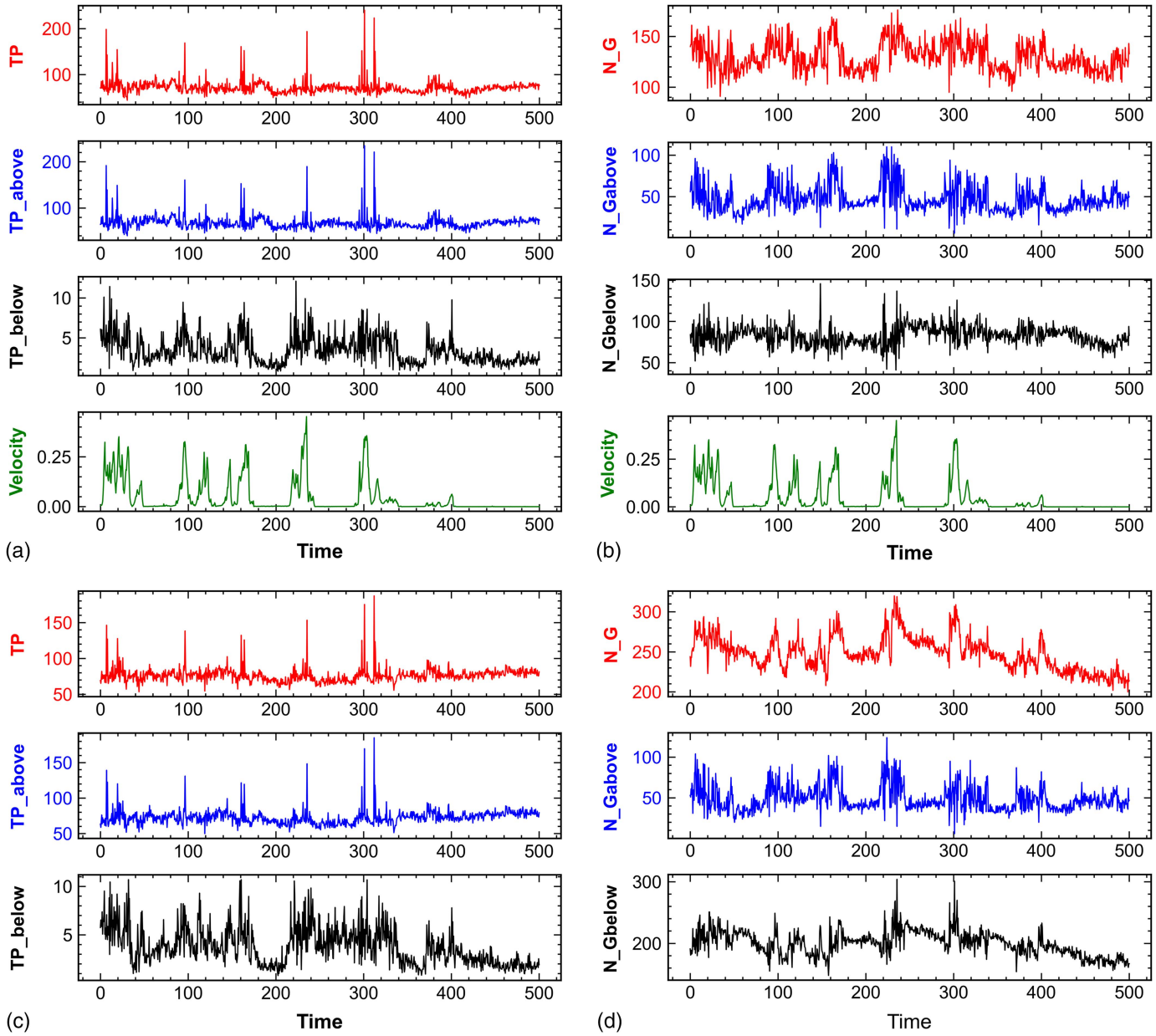

Fig. 7. Disks with basal friction, β_0 (components); total persistence (TP), and number of generators, N_G, for the force contact network (FC) and the force particle network (FP). The bottom plot in (a) and (b) shows the magnitude of the intruder's velocity [the velocity plots in (a) and (b) are identical and are replotted for the ease of comparison with the force network results]. One unit of time in this and the following figures correspond to $1000\delta t$: (a) FC, TP; (b) FC, N_G; (c) FP, TP; (d) FP, N_G.

J. Eng. Mech., 2021, 147(11): 04021100

parameters that we used, the intruder exhibited stick-slip dynamics. Then we proceed with briefly considering the same particle shapes and ϕ values but without basal friction. Such systems experience clogging-type dynamics (continuous intruder motion interrupted only by occasional short stick events). These four considered systems, therefore, differ by both particle shape and type of dynamics.

Results for Disks with Basal Friction

We start by considering disks with basal friction, measuring the total persistence and the number of generators in the PDs, as discussed in the methods section. Both measures were considered for all force thresholds and were also considered separately for the forces with the birth coordinates above (TP_{above}) and below (TP_{below}) the mean force (similarly for N_G). All measures were considered for both FC and FP networks and for both the components (β_0) and the loops (β_1). In each figure, we also plotted the magnitude of the intruder's velocity to facilitate the comparison between the PH-derived measures and the intruder dynamics.

Fig. 7 shows TP and N_G for the FC and FP networks. The motion of the intruder always leads to significant changes for both TP and N_G. The TP results, shown in Figs. 7(a and c), appear to display similar behavior for the FC and FP networks; however, the generators appear to behave differently. A similar conclusion is obtained when we consider the results for loops, shown in Fig. 8. Furthermore, we notice that N_G is significantly larger than the number of points that can be seen on the PDs for the force network snapshots (see Fig. 6). A natural question is, "What is the source of these differences?"

Detailed inspection reveals that a significant number of generators is located at rather small forces and/or very close to the diagonal. These generators correspond to the features that may be due to the small variations of the forces between the particles. In experiments, such features may be very difficult to detect and can be thought of as experimental noise. In experiments or simulations they may correspond to the contacts that are very weak (such as in the case of rattler particles) or that correspond to minor force

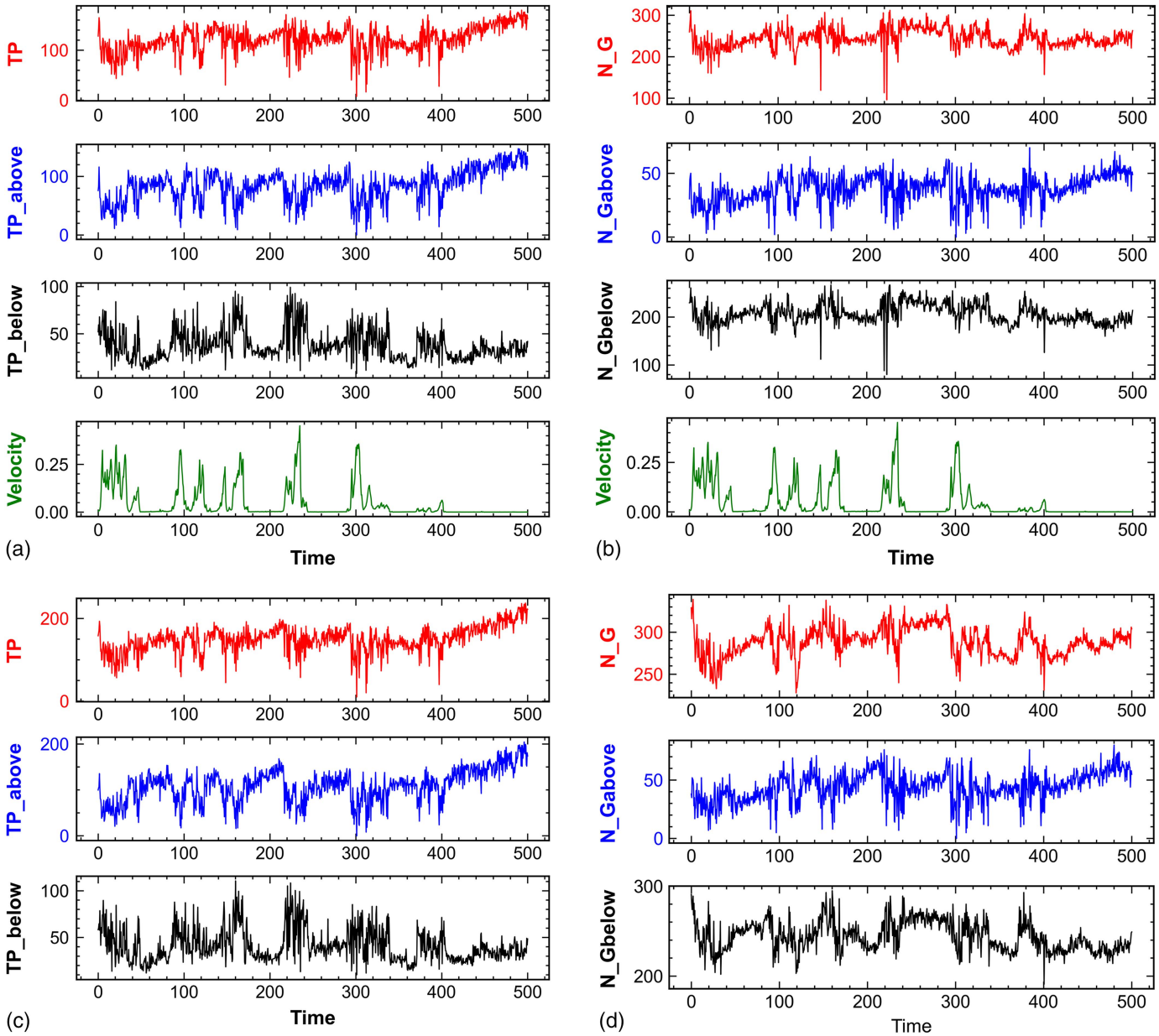

Fig. 8. Disks with basal friction, β_1 (loops): (a) FC, TP; (b) FC, N_G; (c) FP, TP; (d) FP, N_G.

J. Eng. Mech., 2021, 147(11): 04021100

variations. As pointed out previously, these generators do not have strong influence on TP, because they are characterized by very small lifespans. To analyze the significant features characterized by the generators that are further away from the diagonal, we next consider the results obtained by removing a narrow band of thickness δ of the generators that are very close to the diagonal. Figs. 9 and 10 show the corresponding results, where $\delta = 0.1$ (that is, 10% of the mean force). As expected, we find that the TP results are similar to what they would be if the band of generators was not removed, while the number of generators is significantly smaller, in particular for loops and small forces. Table 1 shows the average of the results as δ is varied and also for the case when only very weak forces are removed (birth coordinates less than 10% of the mean force). The results in the table show only relatively minor changes in TP but a dramatic decrease in N_G for both FC and FP networks. This decrease is not influenced strongly by the particular value given to δ, suggesting that most of the removed generators are very close to diagonal. The difference in the results in Columns 0.1 and 0.1^* illustrates how many generators appear for forces weaker than 10% of the mean.

The visual comparison of the figures presented in the foregoing appears promising in the sense that the two considered networks appear similar. To quantify this observation, we computed the (Pearson's) correlation coefficient C between the time series defined by the TP data for the FP and FC networks and separately computed the correlation between the time series defined by the N_G data; for all sets of data, their respective means were subtracted. These calculations were carried out for eight sets of simulations such as the ones shown in Figs. 7–10. To help interpret the results discussed subsequently, note that $C = 1$ means a perfect correlation, $C = 0$ means no correlation, and $C = -1$ means anticorrelation.

Table 2 shows the results. The results for TP show very good correlation, which is not influenced significantly by the removal of the generators close to the diagonal. For the number of generators N_G, we observe significant improvement in the correlation after

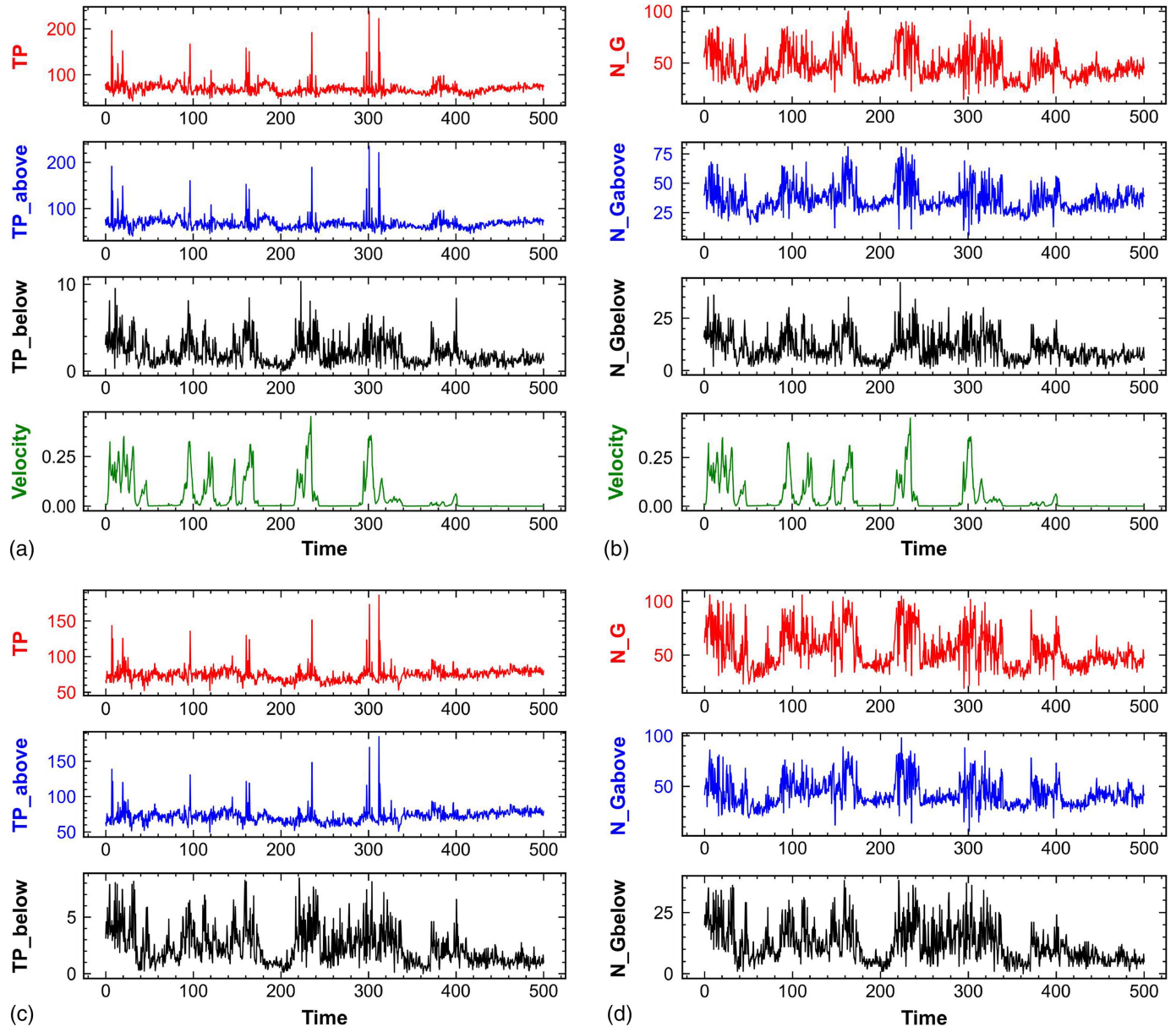

Fig. 9. Disks with basal friction, β_0 (components) after removing the band next to the diagonal ($\delta = 0.1$); compare Fig 7: (a) FC, TP; (b) FC, N_G; (c) FP, TP; (d) FP, N_G.

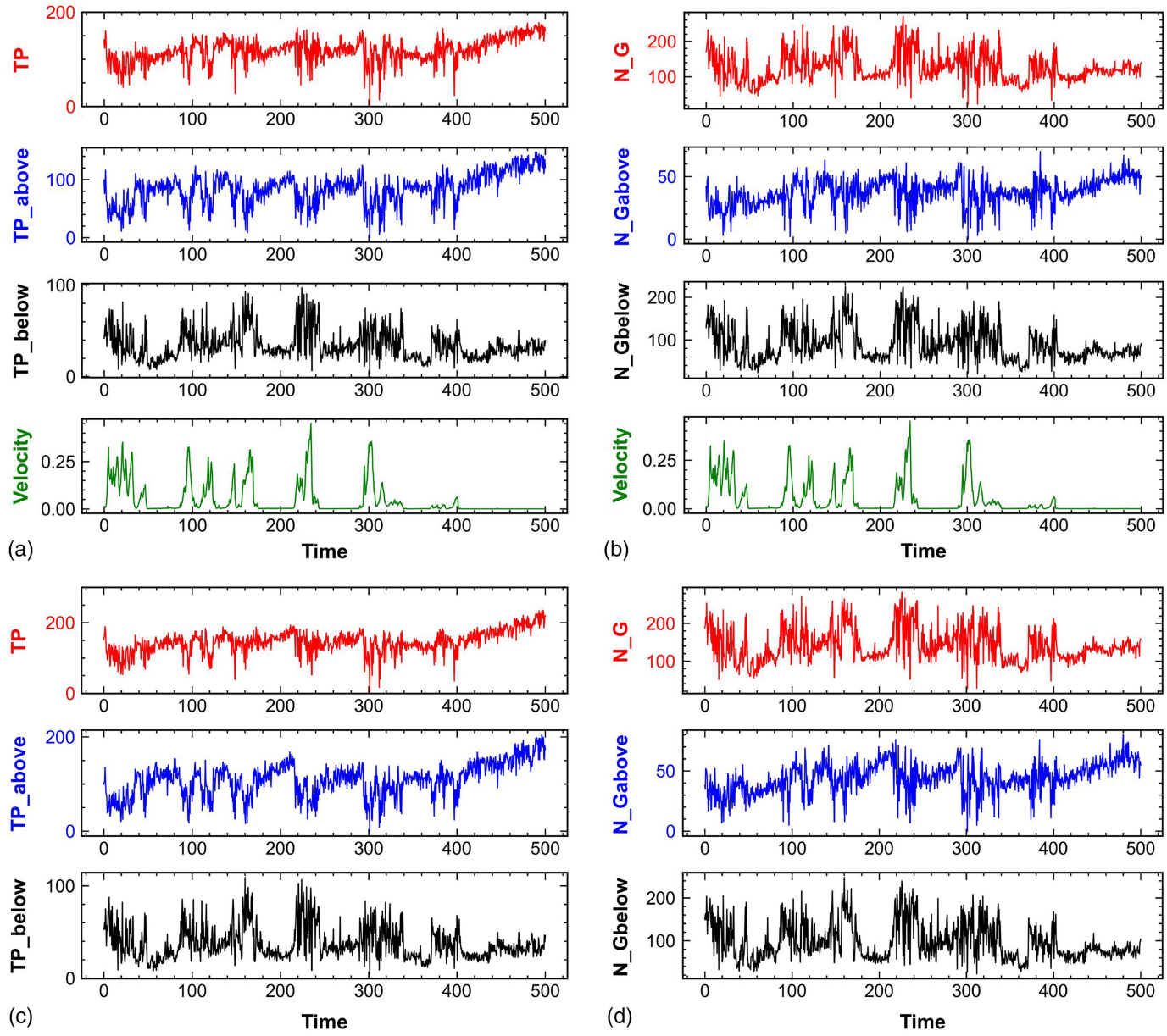

Fig. 10. Disks with basal friction, β_1 (loops) after removing the band next to the diagonal ($\delta = 0.1$); compare Fig 8: (a) FC, TP; (b) FC, N_G; (c) FP, TP; (d) FP, N_G.

Table 1. Average of TP and N_G results obtained after removing a band of generators from persistence diagrams of width δ

		β_0					β_1				
δ		0	0.05	0.1	0.1*	0.2	0	0.05	0.1	0.1*	0.2
FC	TP	94	86	85	86	83	158	148	145	145	140
	TP_{above}	90	83	83	83	82	112	105	105	105	105
	TP_{below}	3.7	3	2	3	1	47	43	40	40	36
	N_G	156	65	53	97	40.5	363	309	148	148	119
	N_{Gabove}	99	46	42	53.7	36	48	47	47	47	47
	N_{Gbelow}	56	19	11	43.7	4	315	236.3	101	101	73
FP	TP	79	76	75	76	73	196	171	169	169	165
	TP_{above}	75	73	73	73	72	143	127	127	127	127
	TP_{below}	4	3.2	2.4	3.6	1.3	53	45	42.5	42.5	38
	N_G	236	70	57	94	44	364	188	160	160	129
	N_{Gabove}	51	48	45	50	39	57	52	52	127	52
	N_{Gbelow}	184	23	12	44	5	307	136	108	42.5	77

Note: Results marked with an asterisk were obtained by removing only the generators with a birth coordinate less than 0.1. All forces were normalized by the mean force.

Table 2. Correlation between topological measures for disks with basal friction shown in Figs. 7 and 8

	β_0				β_1			
δ	0	0.05	0.1	0.2	0	0.05	0.1	0.2
TP	0.86	0.86	0.92	0.92	0.95	0.94	0.94	0.94
TP_{above}	0.85	0.87	0.92	0.93	0.93	0.93	0.95	0.95
TP_{below}	0.91	0.87	0.87	0.87	0.97	0.97	0.97	0.97
N_G	0.42	0.92	0.92	0.92	0.80	0.96	0.96	0.99
N_{Gabove}	0.65	0.90	0.90	0.90	0.76	0.95	0.95	0.95
N_{Gbelow}	0.50	0.80	0.80	0.81	0.78	0.98	0.98	0.98

removing a band of generators. The relatively minor differences between the results as the width of the band is varied suggests that it is important only to remove the generators very close to the diagonal in order to obtain good correlation between the two networks.

Results for Disks without Basal Friction and for Pentagons Other Systems

Here, we briefly discuss three other systems corresponding to different parameter choices: disks without basal friction and pentagons with and without basal friction. As specified previously, for disks we always considered $\phi = 0.78$, and for pentagons we considered $\phi = 0.62$. With basal friction, both systems showed stick-slip dynamics in simulations and experiments; without basal friction the systems exhibited clogging-type dynamics (Carlevaro et al. 2020; Kozlowski et al. 2019). Therefore, by considering the four outlined configurations, we are in a position to discuss both the influence of particle shape and particle dynamics on the force networks and, in particular, on the degree of agreement between the FC and FP networks. Motivated by the high degree of correlation found for disks with basal friction when a narrow band of generators close to the diagonal was removed, we report only such results in the following; furthermore, for brevity we show time series of the results for TP and N_G for pentagons with basal friction only.

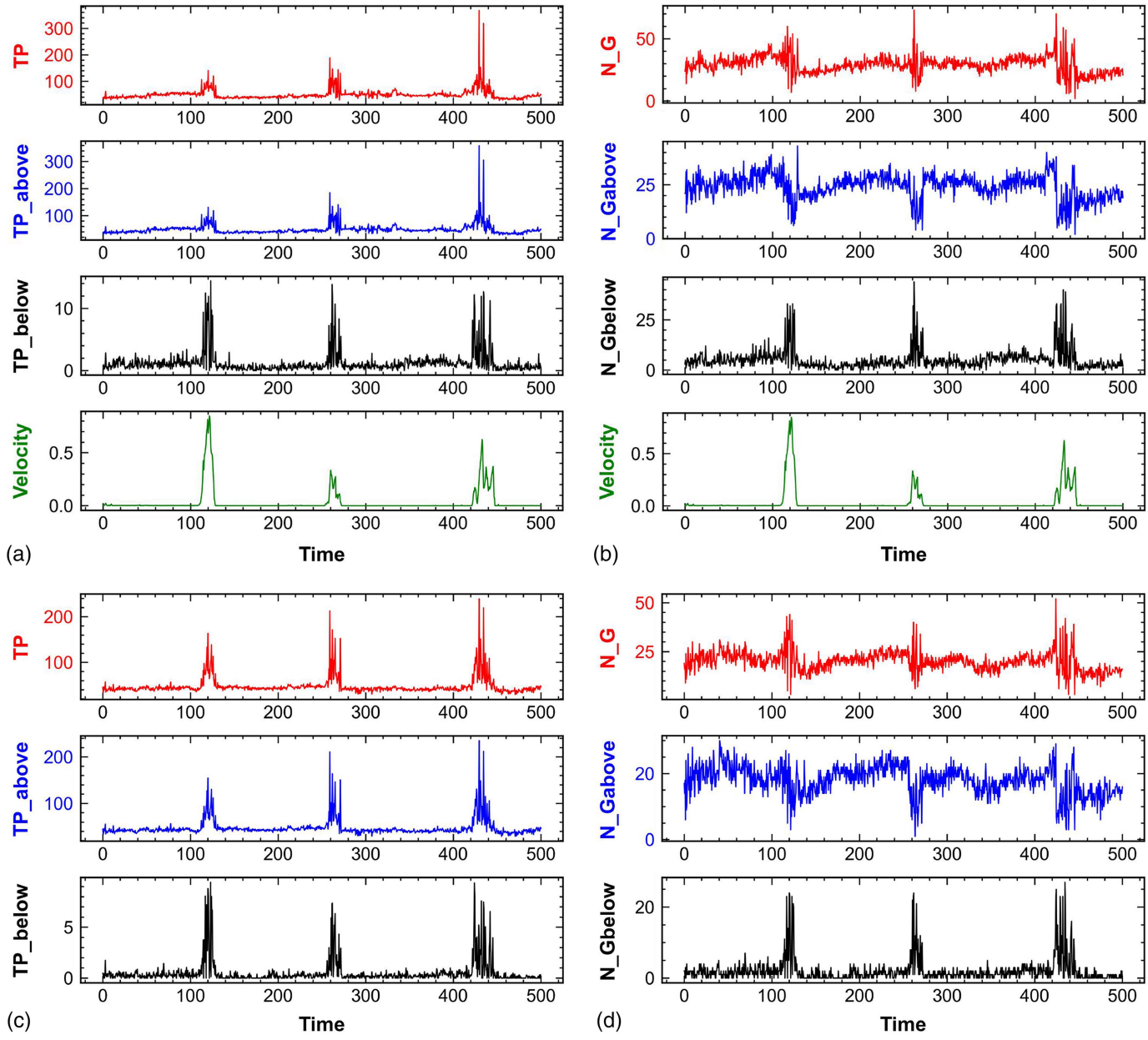

Fig. 11. Pentagons with basal friction, β_0 (components): (a) FC, TP; (b) FC, N_G; (c) FP, TP; (d) FP, N_G.

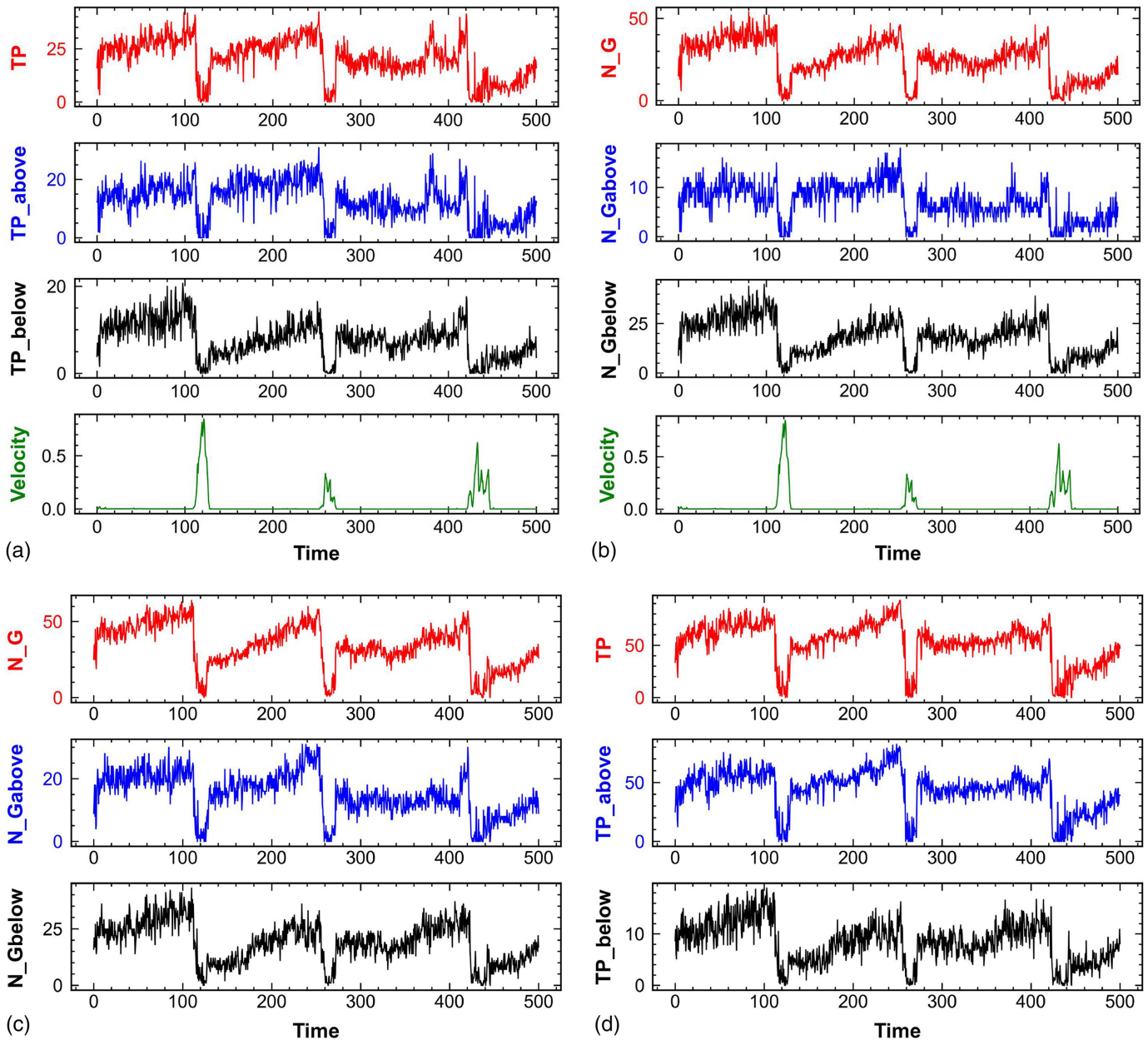

Fig. 12. Pentagons with basal friction, β_1 (loops): (a) FC, TP; (b) FC, N_G; (c) FP, TP; (d) FP, N_G.

Figs. 11 and 12 show the results for pentagons. The comparison with the results for disks shows that the measures that we considered (TP and N_G) were considerably different between the two systems, despite the fact that both systems displayed stick-slip dynamics. For pentagons we observe that the results for TP and N_G were much less noisy, with clearly defined slip events and not many changes in TP during the stick phases. A comparison of the results for the loops (Figs. 10 and 12) is interesting as well. The pentagons show a significantly smaller number of loops. This feature will be discussed in more detail in future work. For our present purposes, the main question was whether the correlation between the FC and FP networks was as good as was found for the disks. Table 3 shows that this was indeed the case; the correlation between the two measures that we considered was still excellent.

Finally, we comment briefly on the results obtained without basal friction. In such systems, one finds clogging type of dynamics, leading to PH results that are much more noisy for both disks and pentagons (not shown for brevity). However, despite the noisy behavior, the correlations between the considered measures, shown in Tables 4 and 5, were still excellent. This suggests that even for dynamic systems, one can still obtain an excellent understanding regarding the evolving force networks even if only total force

Table 3. Correlation between topological measures for pentagons with basal friction shown in Figs. 11 and 12

Measure	β_0	β_1
TP	0.86	0.92
TP_{above}	0.86	0.85
TP_{below}	0.90	0.85
N_G	0.84	0.97
N_{Gabove}	0.81	0.84
N_{Gbelow}	0.86	0.91

Note: This table and the following tables and figures report results obtained after removing the band of generators (of width $\delta = 0.1$) next to the diagonal of the PDs, as discussed in the text.

Table 4. Correlation between topological measures for disks without basal friction

Measure	β_0	β_1
TP	0.85	0.93
TP_{above}	0.83	0.88
TP_{below}	0.80	0.95
N_G	0.89	0.98
N_{Gabove}	0.86	0.94
N_{Gbelow}	0.80	0.95

Table 5. Correlation between topological measures for pentagons without basal friction

Measure	β_0	β_1
TP	0.78	0.87
TP_{above}	0.78	0.74
TP_{below}	0.80	0.83
N_G	0.85	0.92
N_{Gabove}	0.85	0.75
N_{Gbelow}	0.85	0.88

(the magnitude of the forces acting on the particles) is known. Of course, we have considered only one particular setup and only relatively crude measures for the purpose of quantifying the considered networks; further research should consider other types of dynamics as well as more detailed measures for analysis of the considered networks and associated persistence diagrams.

Conclusions

While force networks and their static and dynamic properties are known to be a crucial factor in determining the macroscopic behavior of particulate-based systems, they are difficult to extract from experiments. In this work, we have shown that the topological properties measured by the persistent homology of networks based on complete data versus the ones obtained by incomplete data (which are easier to access in experiments) are similar. This was found to hold for different particle shapes (disks and pentagons were considered) and for stick-slip and clogging-type dynamics.

Furthermore, the presented results set the stage for comparing the results of simulations (for which we have complete data about interparticle forces available) and experiments (for which only partial information may be available). Such a comparison will be the subject of future work.

Data Availability Statement

All the data used in this study are available from the authors upon request.

Acknowledgments

This study was supported by US Army Research Office Grant No. W911NF1810184. Authors L. A. P. and C. M. C. acknowledge support from Universidad Tecnológica Nacional through Grant Nos. PID-MAUTNLP0004415 and PID-MAIFIBA0004434TC and from Consejo Nacional de Investigaciones Científicas y Técnicas (Argentina) (CONICET) through Grant Nos. RES-1225-17 and PUE 2018 229 20180100010 CO.

Supplemental Materials

The animations of the force networks shown in Fig. 5 and corresponding persistence diagrams for Fig. 6 are available online in the ASCE Library (www.ascelibrary.org).

References

Ardanza-Trevijano, S., I. Zuriguel, R. Arévalo, and D. Maza. 2014. "Topological analysis of tapped granular media using persistent homology." *Phys. Rev. E* 89 (5): 052212. https://doi.org/10.1103/PhysRevE.89.052212.

Arévalo, R., L. A. Pugnaloni, I. Zuriguel, and D. Maza. 2013. "Contact network topology in tapped granular media." *Phys. Rev. E* 87 (2): 022203. https://doi.org/10.1103/PhysRevE.87.022203.

Arévalo, R., I. Zuriguel, and D. Maza. 2010. "Topology of the force network in jamming transition of an isotropically compressed granular packing." *Phys. Rev. E* 81 (4): 041302. https://doi.org/10.1103/PhysRevE.81.041302.

Azéma, E., and F. Radja. 2012. "Force chains and contact network topology in sheared packings of elongated particles." *Phys. Rev. E* 85 (3): 031303. https://doi.org/10.1103/PhysRevE.85.031303.

Bassett, D. S., E. T. Owens, K. E. Daniels, and M. A. Porter. 2012. "Influence of network topology on sound propagation in granular materials." *Phys. Rev. E* 86 (4): 041306. https://doi.org/10.1103/PhysRevE.86.041306.

Behringer, R. P., and B. Chakraborty. 2018. "The physics of jamming for granular materials: a review." *Rep. Progress Phys.* 82 (1): 012601. https://doi.org/10.1088/1361-6633/aadc3c.

Bo, L., R. Mari, C. Song, and H. A. Makse. 2014. "Cavity method for force transmission in jammed disordered packings of hard particles." *Soft Matter* 10 (37): 7379–7392. https://doi.org/10.1039/C4SM00667D.

Carlevaro, C., and L. Pugnaloni. 2011. "Steady state of tapped granular polygons." *J. Stat. Mech.* 2011 (01): P01007. https://doi.org/10.1088/1742-5468/2011/01/P01007.

Carlevaro, C. M., R. Kozlowski, L. A. Pugnaloni, H. Zheng, J. E. S. Socolar, and L. Kondic. 2020. "Intruder in a two-dimensional granular system: Effects of dynamic and static basal friction on stick-slip and clogging dynamics." *Phys. Rev. E* 101 (1): 012909. https://doi.org/10.1103/PhysRevE.101.012909.

Catto, E. 2005. "Iterative dynamics with temporal coherence." Accessed March 15, 2017. https://box2d.org/downloads/.

Cheng, C., A. Zadeh, and L. Kondic. 2021. "Correlating the force network evolution and dynamics in slider experiments." Preprint, submitted January 13, 2021. https://arxiv:2101:07218.

Daniels, K. E., J. E. Kollmer, and J. G. Puckett. 2017. "Photoelastic force measurements in granular materials." *Rev. Sci. Instrum.* 88 (5): 051808. https://doi.org/10.1063/1.4983049.

Dijksman, J. A., L. Kovalcinova, J. Ren, R. P. Behringer, M. Kramár, K. Mischaikow, and L. Kondic. 2018. "Characterizing granular networks using topological metrics." *Phys. Rev. E* 97 (4): 042903. https://doi.org/10.1103/PhysRevE.97.042903.

Gameiro, M., A. Singh, L. Kondic, K. Mischaikow, and J. F. Morris. 2020. "Interaction network analysis in shear thickening suspensions." *Phys. Rev. Fluids* 5 (3): 034307. https://doi.org/10.1103/PhysRevFluids.5.034307.

Giusti, C., L. Papadopoulos, E. T. Owens, K. E. Daniels, and D. S. Bassett. 2016. "Topological and geometric measurements of force-chain structure." *Phys. Rev. E* 94 (3): 032909. https://doi.org/10.1103/PhysRevE.94.032909.

GUDHI. 2014. "Topological data analysis and geometric inference in higher dimension." Accessed December 15, 2020. https://gudhi.inria.fr.

Howell, D., R. P. Behringer, and C. Veje. 1999. "Stress fluctuations in a 2D granular Couette experiment: A continuous transition." *Phys. Rev. Lett.* 82 (26): 5241. https://doi.org/10.1103/PhysRevLett.82.5241.

Kawamoto, R., E. Andò, G. Viggiani, and J. E. Andrade. 2018. "All you need is shape: predicting shear banding in sand with LS-DEM."

J. Mech. Phys. Solids 111 (Feb): 375–392. https://doi.org/10.1016/j.jmps.2017.10.003.

Kondic, L., A. Goullet, C. O'Hern, M. Kramar, K. Mischaikow, and R. Behringer. 2012. "Topology of force networks in compressed granular media." *Europhys. Lett.* 97 (5): 54001. https://doi.org/10.1209/0295-5075/97/54001.

Kondic, L., M. Kramár, L. A. Pugnaloni, C. M. Carlevaro, and K. Mischaikow. 2016. "Structure of force networks in tapped particulate systems of disks and pentagons. II. Persistence analysis." *Phys. Rev. E* 93 (6): 062903. https://doi.org/10.1103/PhysRevE.93.062903.

Kozlowski, R., C. M. Carlevaro, K. E. Daniels, L. Kondic, L. A. Pugnaloni, J. E. S. Socolar, H. Zheng, and R. P. Behringer. 2019. "Dynamics of a grain-scale intruder in a two-dimensional granular medium with and without basal friction." *Phys. Rev. E* 100 (3): 032905. https://doi.org/10.1103/PhysRevE.100.032905.

Kramár, M., A. Goullet, L. Kondic, and K. Mischaikow. 2013. "Persistence of force networks in compressed granular media." *Phys. Rev. E* 87 (4): 042207. https://doi.org/10.1103/PhysRevE.87.042207.

Kramár, M., A. Goullet, L. Kondic, and K. Mischaikow. 2014a. "Evolution of force networks in dense particulate media." *Phys. Rev. E* 90 (5): 052203. https://doi.org/10.1103/PhysRevE.90.052203.

Kramár, M., A. Goullet, L. Kondic, and K. Mischaikow. 2014b. "Quantifying force networks in particulate systems." *Phys. D* 283 (Aug): 37–55. https://doi.org/10.1016/j.physd.2014.05.009.

Kramár, M., R. Levanger, J. Tithof, B. Suri, M. Xu, M. Paul, M. F. Schatz, and K. Mischaikow. 2016. "Analysis of Kolmogorov flow and Rayleigh–Bénard convection using persistent homology." *Phys. D* 334 (Nov): 82–98. https://doi.org/10.1016/j.physd.2016.02.003.

Li, L., E. Marteau, and J. E. Andrade. 2019. "Capturing the inter-particle force distribution in granular material using LS-DEM." *Granular Matter* 21 (43): 1–16.

Liu, J., A. Wautier, S. Bonelli, F. Nicot, and F. Darve. 2020. "Macroscopic softening in granular materials from a mesoscale perspective." *Int. J. Solids Struct.* 193 (Jun): 222–238. https://doi.org/10.1016/j.ijsolstr.2020.02.022.

Mileyko, Y., S. Mukherjee, and J. Harer. 2011. "Probability measures on the space of persistence diagrams." *Inverse Prob.* 27 (12): 124007. https://doi.org/10.1088/0266-5611/27/12/124007.

Nicot, F., H. Xiong, A. Wautier, J. Lerbet, and F. Darve. 2017. "Force chain collapse as grain column buckling in granular materials." *Granular Matter* 19 (2): 18. https://doi.org/10.1007/s10035-017-0702-0.

Peters, J., M. Muthuswamy, J. Wibowo, and A. Tordesillas. 2005. "Characterization of force chains in granular material." *Phys. Rev. E* 72 (4): 041307. https://doi.org/10.1103/PhysRevE.72.041307.

Pöschel, T., and T. Schwager. 2005. *Computational granular dynamics: Models and algorithms*. New York. Springer.

Pugnaloni, L., C. Carlevaro, M. Kramár, K. Mischaikow, and L. Kondic. 2016. "Structure of force networks in tapped particulate systems of disks and pentagons. I. Clusters and loops." *Phys. Rev. E* 93 (6): 062902. https://doi.org/10.1103/PhysRevE.93.062902.

Pytlos, M., M. Gilbert, and C. C. Smith. 2015. "Modelling granular soil behaviour using a physics engine." *Geotech. Lett.* 5 (4): 243–249. https://doi.org/10.1680/jgele.15.00067.

Radjai, F., M. Jean, J. J. Moreau, and S. Roux. 1996. "Force distribution in dense two-dimensional granular systems." *Phys. Rev. Lett.* 77 (2): 274–277. https://doi.org/10.1103/PhysRevLett.77.274.

Sarkar, S., D. Bi, J. Zhang, R. P. Behringer, and B. Chakraborty. 2013. "Origin of rigidity in dry granular solids." *Phys. Rev. Lett.* 111 (6): 068301. https://doi.org/10.1103/PhysRevLett.111.068301.

Shah, S., C. Cheng, P. Jalali, and L. Kondic. 2020. "Failure of confined granular media due to pullout of an intruder: from force networks to a system wide response." *Soft Matter* 16 (33): 7685–7695. https://doi.org/10.1039/D0SM00911C.

Snoeijer, J. H., T. J. H. Vlugt, M. van Hecke, and W. van Saarloos. 2004. "Force network ensemble: A new approach to static granular matter." *Phys. Rev. Lett.* 92 (5): 054302. https://doi.org/10.1103/PhysRevLett.92.054302.

Takahashi, T., A. H. Clark, T. Majmudar, and L. Kondic. 2018. "Granular response to impact: Topology of the force networks." *Phys. Rev. E* 97 (1): 012906. https://doi.org/10.1103/PhysRevE.97.012906.

Tighe, B. P., J. H. Snoeijer, T. J. H. Vlugt, and M. van Hecke. 2010. "The force network ensemble for granular packings." *Soft Matter* 6 (13): 2908–2917. https://doi.org/10.1039/b926592a.

Tordesillas, A., S. T. Tobin, M. Cil, K. Alshibli, and R. P. Behringer. 2015. "Network flow model of force transmission in unbonded and bonded granular media." *Phys. Rev. E* 91 (6): 062204. https://doi.org/10.1103/PhysRevE.91.062204.

Tordesillas, A., D. M. Walker, G. Froyland, J. Zhang, and R. Behringer. 2012. "Transition dynamics of frictional granular clusters." *Phys. Rev. E* 86 (1): 011306. https://doi.org/10.1103/PhysRevE.86.011306.

Tordesillas, A., D. M. Walker, and Q. Lin. 2010. "Force cycles and force chains." *Phys. Rev. E* 81 (1): 011302. https://doi.org/10.1103/PhysRevE.81.011302.

Walker, D., and A. Tordesillas. 2012. "Taxonomy of granular rheology from grain property networks." *Phys. Rev. E* 85 (1): 011304. https://doi.org/10.1103/PhysRevE.85.011304.

Zadeh, A. A., et al. 2019. "Enlightening force chains: A review of photoelasticimetry in granular matter." *Granular Matter* 21 (4): 83. https://doi.org/10.1007/s10035-019-0942-2.

Zhao, Y., H. Zheng, D. Wang, M. Wang, and R. P. Behringer. 2019. "Particle scale force sensor based on intensity gradient method in granular photoelastic experiments." *New J. Phys.* 21 (2): 023009. https://doi.org/10.1088/1367-2630/ab05e7.